Sensors & Actuators: A. Physical 365 (2024) 114875

Contents lists available at ScienceDirect

Sensors and Actuators: A. Physical

journal homepage: www.journals.elsevier.com/sensors-and-actuators-a-physical

Piezoelectric wavy whisker sensor for perceiving underwater vortex from a bluff body

Linan Guo, Jianhua Liu, Guitao Wu, Peng Xu, Siyuan Wang, Bo Liu, Yuanzheng Li, Tangzhen Guan, Hao Wang, Jicang Si *, Taili Du *, Minyi Xu *

Dalian Key Lab of Marine Micro/Nano Energy and Self-powered System, Marine Engineering College, Dalian Maritime University, Dalian 116026, China

ARTICLE INFO

Keywords:
Piezoelectric nanogenerators
Bionic seal whisker
Vortex perception

ABSTRACT

Underwater flow field perception is a crucial technique for obtaining the motion status and trajectory of targets. To perceive the vortex in the flow field environment and obtain the disturbance information of the vortex, we propose a piezoelectric wavy whisker sensor (PWWS) inspired by the mechanism of a seal's whisker to perceive and track prey effectively. The PWWS is designed to imitate the unique biological structure of seal whiskers and incorporates the principles of piezoelectric nanogenerators. Specifically, it consists of a waterproof main body made of polydimethylsiloxane (PDMS), and a piezoelectric perceiving unit made of polyvinylidene difluoride (PVDF) encapsulated at the bottom. In the present study, the vortex is generated through a cylinder bluff body. The relationship between the signal of PWWS (peak voltage and frequency) and perception parameters (diameter of the bluff body, distance between the PWWS and the bluff body, impact angle, and flow velocity) are systematically investigated. Then, a mathematical model between vortex parameters and the signal frequency of the PWWS is proposed, and an APP with real-time perception is realized using MATLAB. Through validation by the experimental data, the APP exhibits reasonable predicted results and can well precept the above perception parameters (the error lower than 10%). Therefore, the PWWS has great potential to obtain the motion status and trajectory of underwater targets.

1. Introduction

Currently, the main perception technologies for perceiving underwater environmental features include underwater sonar perception technology[1] and underwater visual recognition technology[2]. Underwater sonar perceiving technology has the characteristic of long perceiving distance, while its effectiveness can be reduced by interference from complex terrain and underwater noise[3]. Underwater visual recognition technology has high-resolution perception and recognition capabilities, but the perception distance is restricted by the visibility of the underwater environment[4]. As marine environments grow increasingly complex due to escalating natural and human-induced disturbances, underwater perception technologies based on acoustics and optics are becoming progressively constrained. Therefore, there is an urgent need to develop new technologies for underwater environmental perception to enhance the perceptual capabilities of underwater environments[5].

Tactile perception, as a new form of underwater environmental perception, can serve as a promising method for underwater environmental target status monitoring [6]. Underwater bionic tactile technology represents a primary area of research, inspired by the ability of underwater creatures to sense changes in their external environment [7–9]. For example, the lateral line system of fish is a tactile sense organ that can perceive tiny fluid movements and pressure gradient changes [10–12]. This natural mechanism has inspired researchers to construct an artificial lateral line array by amalgamating modern pressure sensors and Microelectro Mechanical Systems (MEMS) technology[13]. The experimental results illustrate that this artificial lateral line array is similar to its natural counterpart in evaluating changes in the flow field environment by perceiving changes in pressure through internal sensors [14,15].

Among these, the facial whiskers of seals have received primary attention for their remarkable ability to perceive changes in flow fields caused by external factors[16,17]. Such potential is found by early research of Schulte-Pelkum et al. [18] that seals can detect prey tracks to perceive the environment only by mouth whiskers without relying on

* Corresponding authors.
E-mail addresses: sjc@dlmu.edu.cn (J. Si), dutaili@dlmu.edu.cn (T. Du), xuminyi@dlmu.edu.cn (M. Xu).

https://doi.org/10.1016/j.sna.2023.114875
Received 23 August 2023; Received in revised form 9 November 2023; Accepted 26 November 2023
Available online 29 November 2023

hearing or sight. Adachi et al. [19] subsequently confirmed that seals rely on their whiskers to perceive the flow field disturbances generated by prey to improve tracking efficiency. The structure investigation by Fish et al. [20] demonstrated that elliptical cross-section and the repetitive distribution of peaks and valleys along the whisker's axis are two critical factors that enable seal whiskers to minimize self-disturbance. Lyons et al. [21] demonstrated that the wavy structure of seal whiskers has the effect of reducing hydrodynamic forces as well as modifying vortex-induced vibration response.

In addition, Beem et al. [22] confirmed in their study that the structure of seal whiskers generates significant vibrations in vortex wake. Zheng et al. [23] also obtained the same results in exploring the hydrodynamic effects of the wake of a cylindrical bluff body (similar to the wake of a fish's tail) on the whiskers of seals. Therefore, the unique wavy structure of seal whiskers provides researchers with inspiration for constructing new high-performance structures for sensors. Gul et al. [24] designed a fully 3D printed pinniped inspired cylindrical whisker sensor, which can perceive vortices by analyzing analog signals. Compared to cylindrical whisker sensors, Liu et al. [25] proposed a novel piezoresistive flow sensor, which has a bionic whisker with an undulated morphology. The whisker sensor can reach a detection limit of 8 mm/s when measuring oscillating currents. This also confirms that the wavy structure design can greatly improve perceiving performance, which has aroused great interest among researchers. Beem et al. [26] then designed a single underwater piezoresistive sensor inspired by the special geometric shape of seal whiskers, results demonstrate an improved detection accuracy. To further improve the signal-to-noise ratio and perception accuracy. Zheng et al. [27] proposed a novel piezoresistive bionic seal whisker. This device has high sensitivity and can perceive vortex-induced disturbances that are generated from ten times the diameter upstream of the bionic seal whiskers. However, it relies on an external power source for vortex detection.

Self-powered sensors seem to be attractive alternatives due to their sustainability. Zhang et al. [28] presented a self-powered piezoelectric sensor for Unmanned Underwater Vehicles (UUVs), to sense flow angle of attack and velocity in simple flow field environments. In conducting in-depth research on the perception of fluid characteristics in complex flow field environments, Wang et al. [29] designed an underwater bionic whisker sensor (UBWS) based on a triboelectric nanogenerator with a fast response speed and high signal-to-noise ratio. To our knowledge, there has been no research on the perception of vortex characteristics using piezoelectric bionic whiskers.

In this work, we have designed a piezoelectric wavy whisker sensor (PWWS) with high sensitivity and great stability based on piezoelectric nanogenerators. Specifically, it consists of a waterproof main body made of polydimethylsiloxane (PDMS), and a piezoelectric perceiving unit made of polyvinylidene difluoride (PVDF) encapsulated at the bottom. The piezoelectric material in the perceiving unit is encapsulated with electrostatic shielding materials to improve the anti-interference performance in the underwater environment.

The present research is carried out experimentally, with numerical simulation validating the experimental finding. Specifically, the effects of flow velocity, diameter of the bluff body, and vortex-shedding distance on the signal output of PWWS are investigated. After analysis of the experimental data, we establish mathematical models that correlate vortex field parameters with the characteristic parameters of the PWWS voltage signal. Finally, the accuracy of the mathematical models is validated through experiments, and the feasibility of the PWWS for vortex perception is demonstrated.

2. Results and discussion

2.1. Structure and fabrication of the PWWS

Seals possess the ability to perceive the wake generated by prey swimming through the whiskers around their mouths, which is a key perception method for hunting in the deep sea. Studies have found the wavy structure of whiskers is most likely crucial for them to perceive flow field disturbances[30]. This unique wavy structure can reduce the disturbance of the whiskers caused by the seal's movement.

The piezoelectric wavy whisker sensor is designed by imitating the geometric shape of seal's whiskers, with an equal magnification of 10 times, as shown in Fig. 1a. Specifically, the vertical length of the bionic seal whisker is l= 210 mm, with two major axes of d_1 = 15.0 mm and d_2 = 12.0 mm, and the minor axis of d_1'= 7.5 mm and d_2'= 6 mm. (The details of the structural design are shown in Fig. S1). Fig. 1b illustrates the internal structure of the perceiving unit used in the PWWS.

Specifically, PWWS consists of two parts: a piezoelectric perceiving unit and the main body. A piezoelectric perceiving unit is sealed at the bottom of the PWWS, which can generate electrical signals when external pressure fluctuates. This piezoelectric perceiving unit is made of polyvinylidene difluoride (PVDF) with a thickness of 52 μm and an area of 30 mm × 10 mm. The conductive silver (Ag) paste is deposited on the surface on both sides of PVDF by metal screen printing technology (Fig. S2). Then, the PVDF is encapsulated with cast polypropylene (CPP) tape and implanted into the bottom of the PWWS (Fig. S3). Fig. 1c shows the Scanning electron microscope (SEM) photos of silver paste printed on the PVDF surface at 20.0 kx and 40.0 kx magnification. As shown in the photos, conductive silver particles are in the form of flakes and fish scales. The surface-to-surface contact between fish scale-like particles exhibits excellent conductivity. Supplementary SEM photos are shown in Fig. S4.

The fabrication of the main body consists of the following steps, as shown in Fig. 1d:

(I) Preparing the solution of the main body. The main body of the PWWS is made of PDMS (SYLGARD 184 silicone elastomer). The solution of the main body is mixed by using the main agent and curing agent in a mass ratio of 9:1 (27 g:3 g).
(II) Mixing the solution. The mixed solution is placed and stirred on the surface of a magnetic stirrer at 800 rpm for 5 min. The mixed solution is subsequently placed in a vacuum-drying oven and placed in a negative pressure environment of 0.04Mpa for 3 min to eliminate bubbles generated during the stirring process.
(III) Pouring the solution into the mold for molding. The solution is stewed at room temperature for 10 min, drained with a glass rod, and slowly poured into the resin mold supported by 3D printing technology. A prepared piezoelectric perceiving unit is placed into the mold. The mold is then placed in a vacuum-drying oven with a negative pressure environment of 0.04Mpa for 3 min to eliminate finer bubbles.
(IV) Heating and drying. After another 10 min of standing, the mold is placed into a dry oven under 45 ℃ for 2 h to be de-molded.

2.2. Theories of the PWWS

2.2.1. Theories of the vortex shedding

When a uniform incoming flow with a velocity above a certain value flows through a bluff body, a periodic shedding vortex is generated. This phenomenon can cause objects located in the vortex wake region to oscillate regularly. Specifically, the relationship between the shedding frequency of vortex and flow velocity follows the Strouhal relationship:

$$f = S_t \times \frac{U}{L} \tag{1}$$

where f is the vortex shedding frequency; S_t is Strouhal number; U is the velocity of flow; L is the maximum cross-sectional diameter of the bluff body.

Strouhal number is mainly related to the Reynolds number. Therefore, the Strouhal number and Reynolds number are often used as the main parameters to characterize vortex shedding. According to David

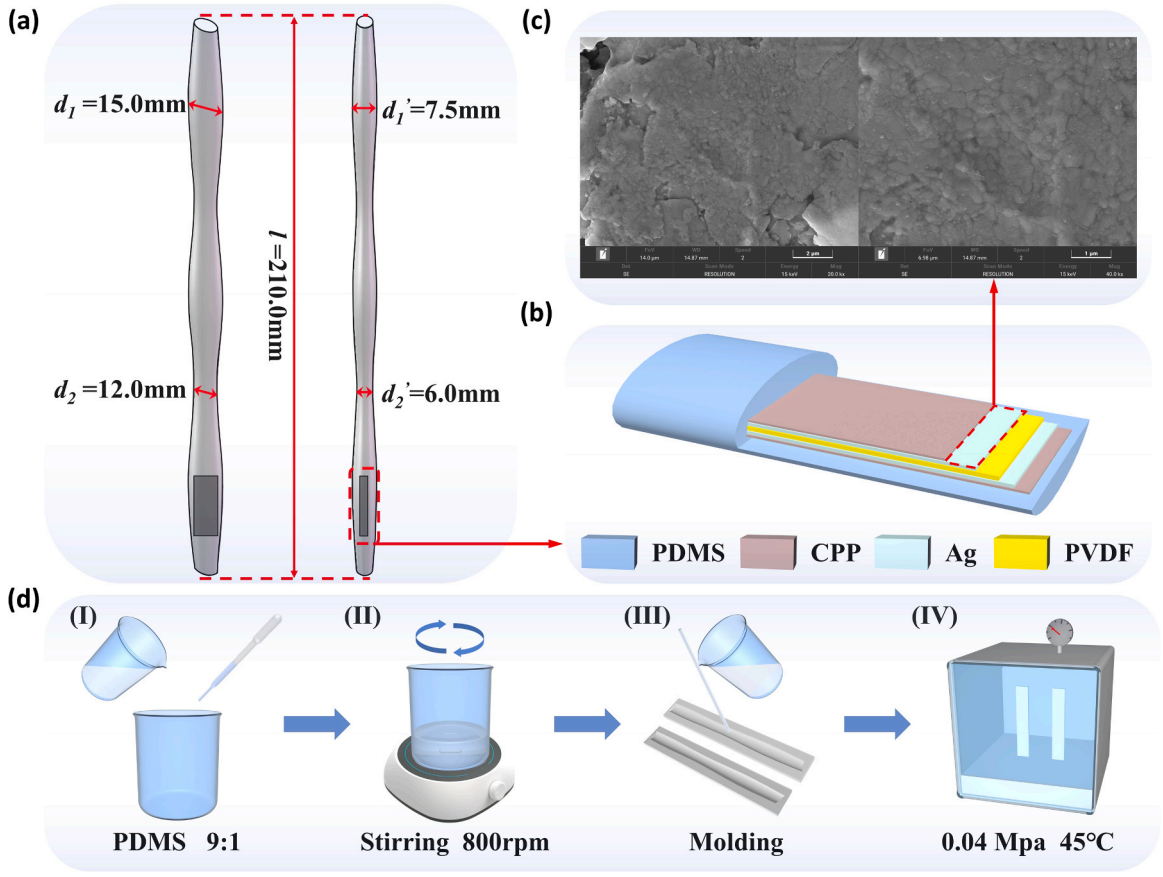

Fig. 1. The structure design and the fabrication of the piezoelectric wavy whisker sensor. (a) The structure and the parameters of the PWWS. (b) The internal structure of the piezoelectric perceiving unit. (c) Scanning electron microscope (SEM) photos of silver electrodes on the PVDF surface at 20.0 kx and 40.0 kx magnification. (d) The fabrication of the PWWS.

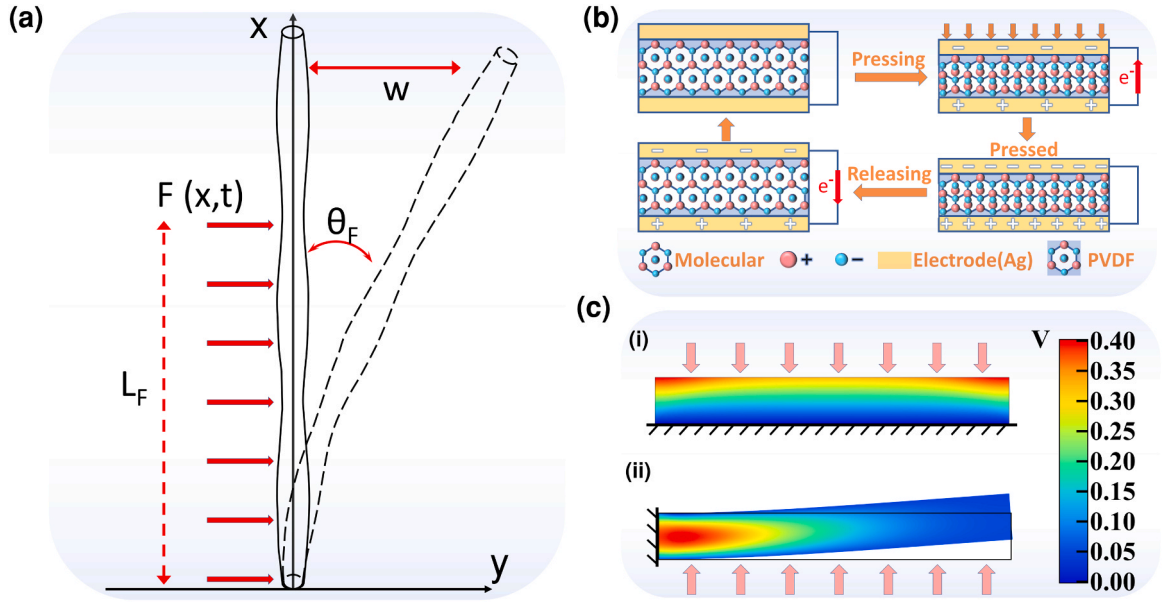

Fig. 2. Theories of the PWWS. (a) Schematic of the deflection of the PWWS by a force. (b) The working cycle of electrical signals generated by the piezoelectric perceiving unit. (c) The simulation diagram of piezoelectric voltage generated inside PVDF materials under different constraint conditions when subjected to external forces.

et al.'s work[31], their relationship is:

$$R_e = \frac{\rho U L}{v} \tag{2}$$

$$S_t = \frac{2fA}{U} \tag{3}$$

where ρ is the water density; L is the diameter of the cross-sectional of a bluff body; v is the dynamic viscosity of water; $2A$ is the width of the wake. In the subcritical region of the vortex where $R_e < 3 \times 10^5$ (for flow around a circular cylinder), the value of Strouhal number is 0.2 (S_t= 0.2).

A model relating the vortex to the force on the PWWS is shown in Fig. S5, where (x_v, y_v) is the coordinate of the vortex center, and *(x,0)* is the coordinate of the stress point. When a vortex flows near the whisker, the pressure difference will cause the whisker to deflect. According to the detailed theory[32,33], the maximum force on the surface of the bionic whisker $F_{\max}$ can be expressed as

$$F_{\max} = \frac{1}{2\pi}\cdot\frac{1}{d} l \rho_f \Gamma \int_0^d \left\{ \frac{u_v}{\sqrt{(x-x_v)^2 + (y_v)^2}} - \frac{1}{4\pi}\cdot\frac{\Gamma}{(x-x_v)^2 + (y_v)^2} \right\} x dx \tag{4}$$

where d is the width of the bionic whisker; l is the length of the whisker; ρ_f is the density of the fluid; Γ is the vortex strength and u_v is the velocity of the vortex center in the x-direction.

2.2.2. The force model of the PWWS

As shown in Fig. 2a, a more detailed model for the deflection of the artificial whisker is presented, where the Euler–Bernoulli undamped whisker model with a uniform cross-section can be expressed as[34].

$$EI\partial^4 w/\partial x^4 + \rho A \partial^2 w/\partial t^2 = F(x,t) \tag{5}$$

where w denotes the whisker's lateral displacement; x is the whisker's axial location; $F(x,t)$ is the external load at time t.

In the following research, we denote the vortex shedding frequency, the impact angle (angle between the direction of fluid flow and the direction of the major diameter of the PWWS, as shown in Fig. S6), the dimensionless number ratio between the diameter of the bluff body and the major diameter of the PWWS, and the dimensionless number distance between the bluff body and the PWWS as f, α, L/d, and D/d. Here, D is the distance between the bluff body and the PWWS, L is the diameter of the bluff body, and d is the major diameter of the PWWS.

2.2.3. Theory of piezoelectricity

The voltage generated by piezoelectric materials under force is mainly influenced by the piezoelectric charge constant d_{ij}. The d_{ij} shows the relationship between the applied mechanical stress and the generated charge, i and j represent the directions of the poled poles and applied force. [35,36] The mode of d_{31} represents the direction of the generated electric signals and is dependent on the direction of the applied force. And the mode of d_{33} represents the direction of the generated electric signals parallel to the direction of the applied force. [37] The open-circuit voltage (V_{oc}) generated when the piezoelectric material is deformed by applied force is shown by

$$V_{oc} = \int g_{33}\varepsilon(l) E dl_3 \tag{6}$$

where g_{33} is the piezoelectric voltage constant ($g_{33} = d_{33}/\varepsilon^T$, ε^Tdenotes the permittivity under a constant strain), $\varepsilon(l)$ is the external strain, E is the elasticity modulus and the integral of l_3 is the distance between the electrodes.

Fig. 2b shows the working cycle of the electrical signal generated by the perceiving unit in the case of a short circuit. When PVDF is subjected to external pressure, its internal molecular structure will produce weak deformation, resulting in the relative displacement of the internal positive and negative charge centers. Therefore, induced charges are generated on the surfaces of the two external electrodes of PVDF, causing electrons to flow from the positive electrode to the negative electrode through an external circuit. As the external force on PVDF reaches its maximum limit, the PVDF and the electrodes on both sides form an electrostatic equilibrium state, resulting in the cessation of electron movement. As external force is gradually removed, the displacement of positive and negative charge centers is reduced, causing electrons to flow from the negative electrode to the positive electrode through the external circuit to reach the initial state.

Fig. 2c presents the simulation of piezoelectric voltage generated inside PVDF materials under different constraint conditions when subjected to external forces. Fig. 2c-(i) and Fig. 2c-(ii) illustrate the distribution of piezoelectric voltage under longitudinal and transverse constraints, respectively. When one end of the piezoelectric material (PVDF) is fixed and subjected to bending deformation under external force, the piezoelectric voltage is mainly concentrated in the bottom region. Therefore, the transverse constraints are adopted for PWWS in the following experiments.

2.3. Experimental equipment

Fig. 3a shows the schematic of the present experiment, consisting of a dragging system, a signal collecting system, a signal analysis system, and an underwater motion capture system. The individual components of the systems are shown in Fig. S7 – S10.

The process of vortex perception is shown in Fig. 3b (I-IV). During the experiments, as the bluff body is dragged in the water, vortices are generated behind and gradually shed. These shedding vortices will stimulate the PWWS to oscillate and generate a voltage signal for the piezoelectric perceiving unit. Such signal is subsequently collected from the collector. These signals are calculated and analyzed for vortex perception in the computer (Fig. 3c). To consistently uniform the motion of both the bluff body and the PWWS, a motor on the dragging guide rail is employed throughout the experiment. Fig. 3d shows a detailed view of the device setup, illustrating the relative positions of the bluff body and the PWWS. To coordinate with the underwater motion capture system and capture the swinging posture of the PWWS, three reflective marking points are arranged on the main body of the PWWS. As the PWWS swings under the influence of bluff body wake, the motion of the reflective marker points will be captured by six underwater motion capture cameras. The live-action of PWWS swinging to different positions under the influence of vortex shedding from the bluff body is depicted in Fig. 3e.

3. Results and discussion

3.1. Output performance of the PWWS

Firstly, we conducted experimental tests on the performance characteristics of the PWWS. Fig. 4a-i and Fig. 4a-ii show the real image of the PWWS from different angles. Fig. 4a-iii shows the image of the perceiving unit. To analyze the sensitivity of the PWWS, the voltage towards various pressures is plotted as shown in Fig. 4b. And the PWWS showed a sensitivity of 0.01796 V/kPa through linear simulation. The voltage signal of the PWWS exhibits great linear change within the pressure from 0 kPa to 50 kPa. After conducting multiple sets of experiments, we synthesized the data to establish the relationship between the peak voltage and v, L/d & D/d, as shown in Fig. 4c. Fig. 4d demonstrates outstanding watertightness of the PWWS, which can still maintain great performance even after soaking in water for 30 days. Moreover, as shown in Fig. 4e, one hundred consecutive experimental cycles were performed under the same experimental conditions, which demonstrates the PWWS has great durability and fast recovery speed

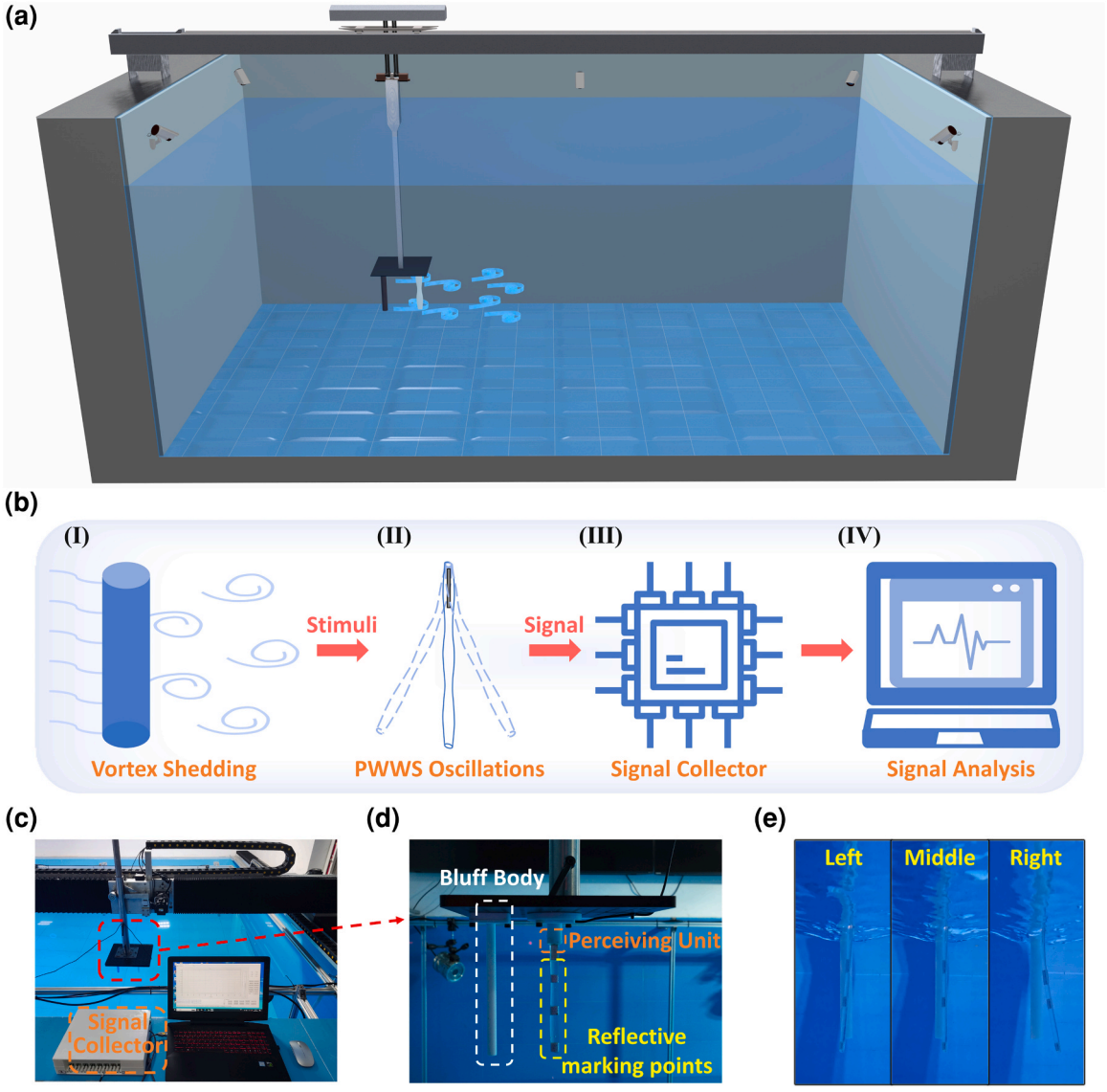

Fig. 3. The equipment and experimental scheme. (a) The equipment and system used in the experiment. (b) Logical diagram (I-IV) showing how the PWWS achieved vortex perception. (c) Partial equipment used in the experiment. (d) Preparation of main experimental devices. (e) Different positions of the PWWS under the influence of vortex shedding from the bluff body.

during continuous work.

Figs. 5a-5c show the Experiment output of the PWWS. Under the condition of L/d = 1.0, D/d = 8, v = 0.4 m/s, as α gradually increased from 0° to 90°, the peak voltage of the PWWS gradually increases from 0.09061 V to 0.21922 V (Fig. 5a). This increment in the peak voltage is attributed to the growing contact area of the PWWS influenced by the vortex, which subsequently enhances the oscillation of the PWWS, increasing its voltage signal. Fig. 5b exhibits the effect of L/d for D/d= 8, v= 0.4 m/s, α = 0°. The results demonstrate an obvious rise in peak voltage as L/d increases. Such phenomena can be explained due to the increase of amplitude in vortex shedding, leading to a larger pressure difference between the PWWS at the same position in the wake region. In addition, the voltage signal period of PWWS gradually expands within the range of L/d from 0.75 to 2.00. This can be explained by Eq. (1) where the increase in L leads to a reduction in the frequency of vortex shedding. In the condition of L/d= 1.0, v= 0.4 m/s, α = 0°, Fig. 5c demonstrates that the peak voltage of the PWWS decreases as D/d gradually increases. This decrease is due to the inherent flow damping of water, leading to a gradual reduction in the pressure difference around the vortex field as the shedding distance increases. The amplitude of the voltage signal generated by its internal piezoelectric unit also decreases as the disturbance force applied to PWWS decreases. However, as shown in Fig. 5c, there is no significant change in the voltage signal period of PWWS when D/d > 6. This can be explained by Eq. (1) as well as Eq. (4) that the distance between the PWWS and the bluff body has little significant effect on the frequency of vortex shedding and vortex intensity decays slowly downstream. Furthermore, the relationship between the voltage signal characteristics of the PWWS and the variation of vortex field parameters is supported by simulation calculations conducted using COMSOL Multiphysics 5.6. Detailed establishment of simulation models and the analysis of simulation data can refer to Fig. S11 and Fig. S12. The simulation results will be discussed in the supporting information. Supplementary Movie 1 and Movie 2 respectively display comparative animations of vortex-shedding states under different conditions.

Supplementary material related to this article can be found online at.

To establish the relationship between the voltage signal of PWWS and variables (impact angle α, L/d, and D/d), more suitable fitting methods are adopted for the experimental data to reduce errors. These relationships are as follows.

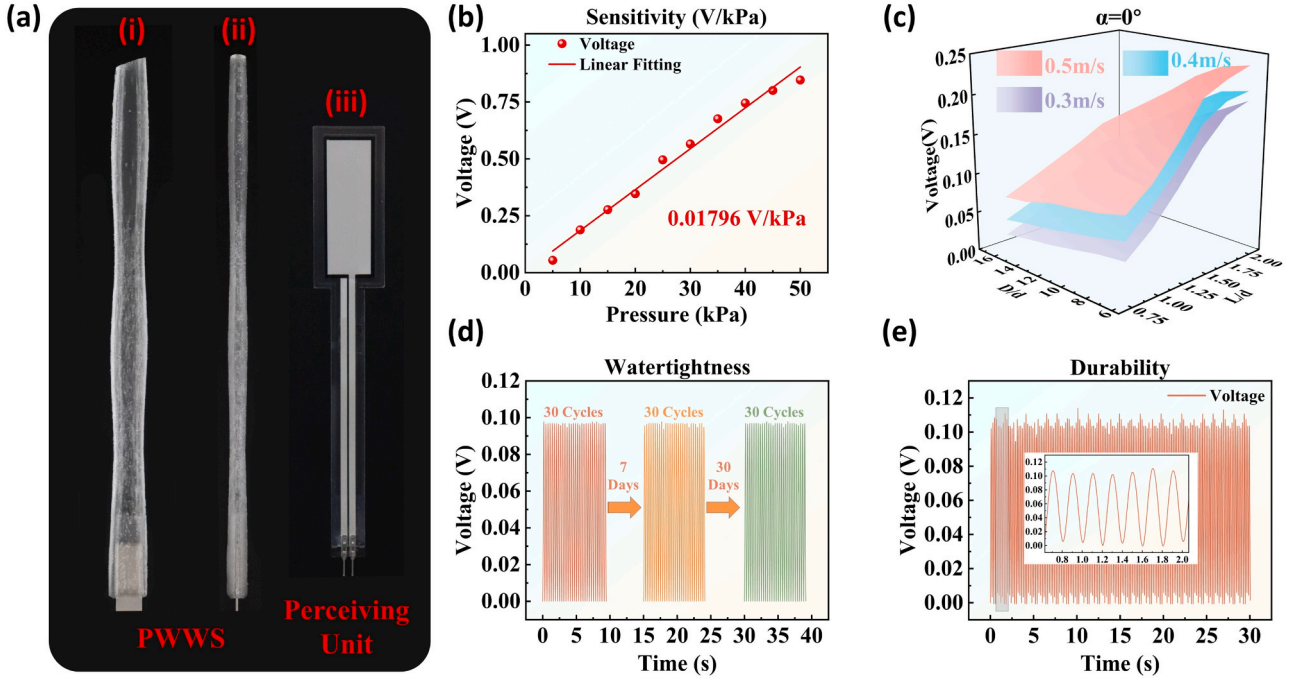

Fig. 4. Performance of the PWWS. (a) Real image of the PWWS and perceiving unit. (b) The voltage towards various pressures. (c) Relationship between the peak voltage of the PWWS, v, D/d, and L/d when α = 0°. (d) Watertightness test of the PWWS. (e) Durability test of the PWWS.

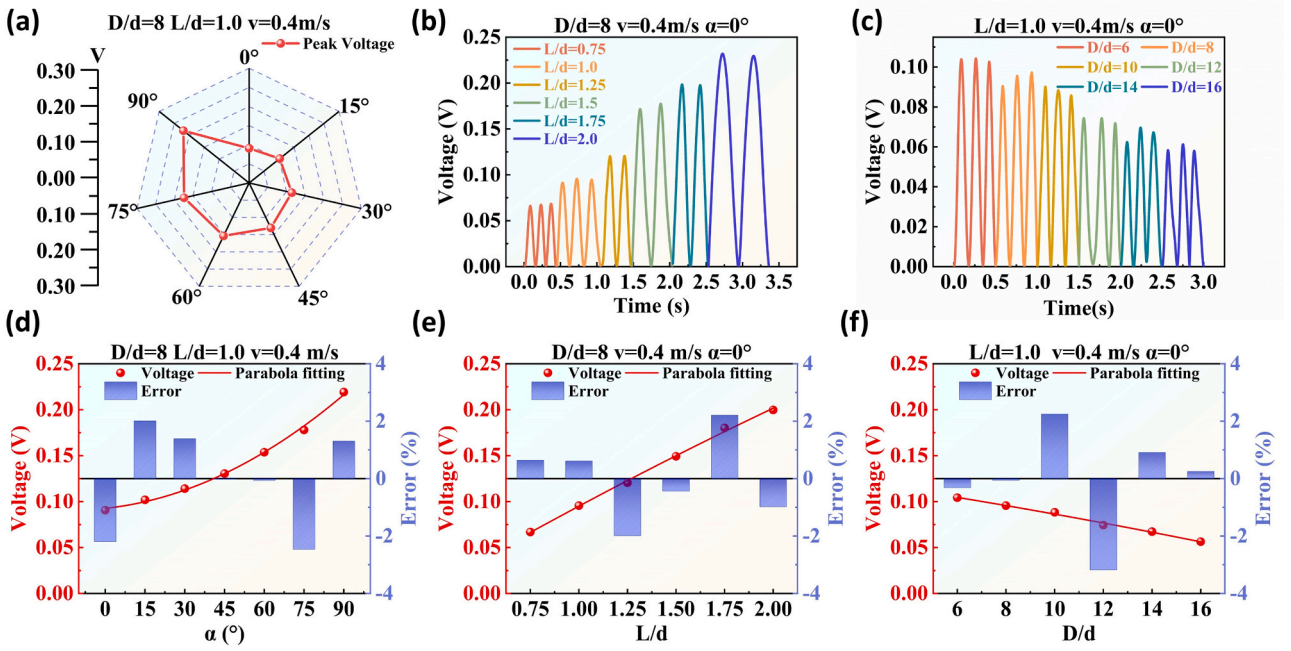

Fig. 5. Output performance of the PWWS. (a) The peak voltage of the signal of the PWWS from the impact angle α = 0–90°. (b) Response performance from L/d= 0.75–2.00. (c) Response performance from D/d= 6–16. (d-f) The error between the voltage signal of the PWWS and the fitted value in the range of (d) α = 0–90°, (e) L/d= 0.75–2.00. (f) D/d= 8–16.

For impact angle:

$$V = 0.0926 + 3.08658 \times 10^{-4} \times \alpha + 1.18487 \times 10^{-5} \times \alpha^2 \quad (7)$$

For L/d:

$$V = -0.01346 + 0.10822 \times \frac{L}{d} \quad (8)$$

For D/d:

$$V = 0.13425 - 0.00484 \times \frac{D}{d} \quad (9)$$

The error of fitting curve versus experimental data are shown in Fig. 5d-f, respectively. The relative errors are below 4%, demonstrating great fitting results.

The relationship between the dominant frequency of signals and the above parameters is further discussed. For D/d= 8, L/d= 1.0, α = 0°, Fig. 6a depicts the corresponding dominant frequency of signals

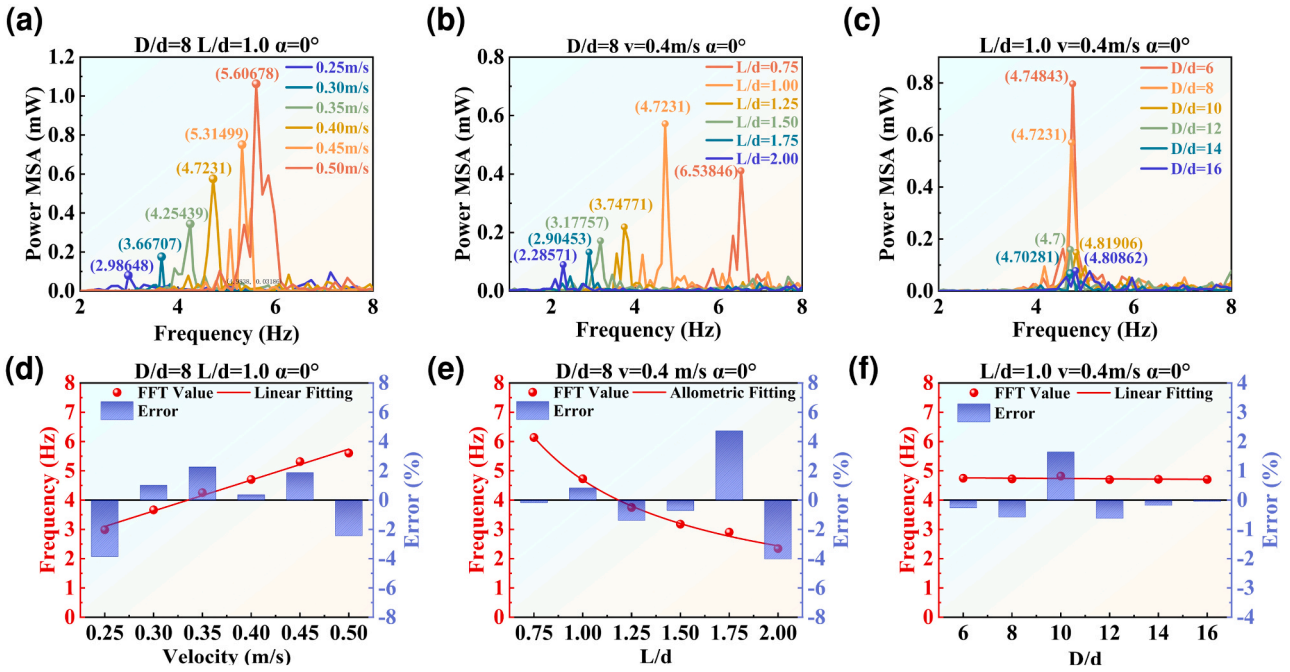

Fig. 6. Deep analysis of experimental data. (a-c) The signal dominant frequency obtained by Fast Fourier transform on the voltage signal of PWWS in the range of (a) v= 0.25–0.50 m/s, L/d= 0.75–2.0, D/d= 6–16. (d-f) The error between the signal dominant frequency of the PWWS and the fitted value in the range of (d) v= 0.25–0.50 m/s, (e) L/d= 0.75–2.00, (f) D/d= 6–16.

obtained through the Fast Fourier transforms on the voltage signal of PWWS at flow velocities ranging from 0.25 to 0.50 m/s. Results demonstrate that the dominant frequency of the PWWS voltage signal rises as flow velocity increases. Similarly, considering the parameters D/d= 8, v= 0.4 m/s, $\alpha = 0°$, Fig. 6b shows the varying dominant frequencies of the PWWS voltage signal within the range of L/d= 0.75–2.00. Notably, the dominant frequency of the PWWS voltage signal diminishes L/d increases. In the range of D/d= 6–16, Fig. 6c shows the signal dominant frequency of the PWWS for the condition of L/d= 1.0, v= 0.4 m/s, $\alpha = 0°$. The dominant frequency of the PWWS signal is relatively stable within the range from 4.7 to 4.81906 as the D/d value increases. All of these can be explained by Eq. (1). As Strouhal number (S_t) is nearly identical, the frequency of vortex shedding is mainly influenced by flow velocity (U), and the diameter of the bluff body (L). According to Figs. 6a-6c, the dominant frequency after the Fourier transform of the voltage signal has a high signal-to-noise ratio, which will facilitate the construction of an accurate and highly applicable mathematical model. The above monotonous trend will be conducive to the establishment of the perception method.

Specifically, the relationship between flow velocity v, L/d, and D/d is fitted using Least Square Fitting individually. These relationships are as follows.

For flow velocity:

$$f = 0.45925 + 10.56828 \times v \tag{10}$$

For L/d:

$$f = 4.68892 \times \left(\frac{L}{d}\right)^{-0.94246} \tag{11}$$

For D/d:

$$f = 4.79275 - 0.0053 \times \frac{D}{d} \tag{12}$$

The error of fitting curve versus experimental data are shown in Fig. 6d-f, respectively. The relative errors are below 5%, demonstrating great fitting results. Moreover, these fitting results can be further proved by Eq. (1) where the frequency is directly proportional to flow velocity while inversely proportional to the diameter of the bluff body, and has no direct relationship with the distance.

This section discusses in detail the changes in amplitude and frequency of the peak voltage signal of PWWS when different parameters (flow velocity v, impact angle α, dimensionless diameter of the bluff body L/d, and the dimensionless distance between the bluff body D/d) are changed. The results indicate that in the experiment, the amplitude and frequency changes of the voltage signal of the PWWS have an ideal monotonic variation with the above variables, and have a great fitting effect (the error is less than 5%). Moreover, these fitting equations can be validated through theory equations. The above experiments demonstrate that the PWWS has great perceptual ability. In the next section, we will further verify the perception ability of the upstream bluff body by the PWWS.

3.2. *Verification of Vortex Perception by the PWWS*

This section aims to comprehensively verify the above perception relationships of PWWS proposed in the previous section. To integrate the perception data of various physical features in the vortex flow, we proposed an APP written by MATLAB suitable for real-time visualization and perception. It can conduct conjoint analysis on the characteristics of the bluff body and the vortex. These analyses are realized by applying the corresponding mathematical relationships with vortex characteristics proposed in Section 3.1. Fig. 7a demonstrates a testing platform for the real-time display function of the APP. The experimental testing process is recorded in Supplementary Movie 3. Fig. 7b shows the record of this test from an underwater perspective. The experimental process recorded from an underwater perspective is shown in Supplementary Movie 4. Fig. 7c shows the interface and functions of the designed APP, including the display of the original signal and the results of parameter estimating. Fig. 7d and Fig. 7e record the main test parameters in this test, including frequency (f), the voltage signal of the PWWS, and distance (D/d). During the experimental process, the mechanical vibration generated during the start and stop of the dragging system will have a large impact on the signal of the PWWS. Therefore, the signals from these two stages do not have reference values. The signal recorded in the

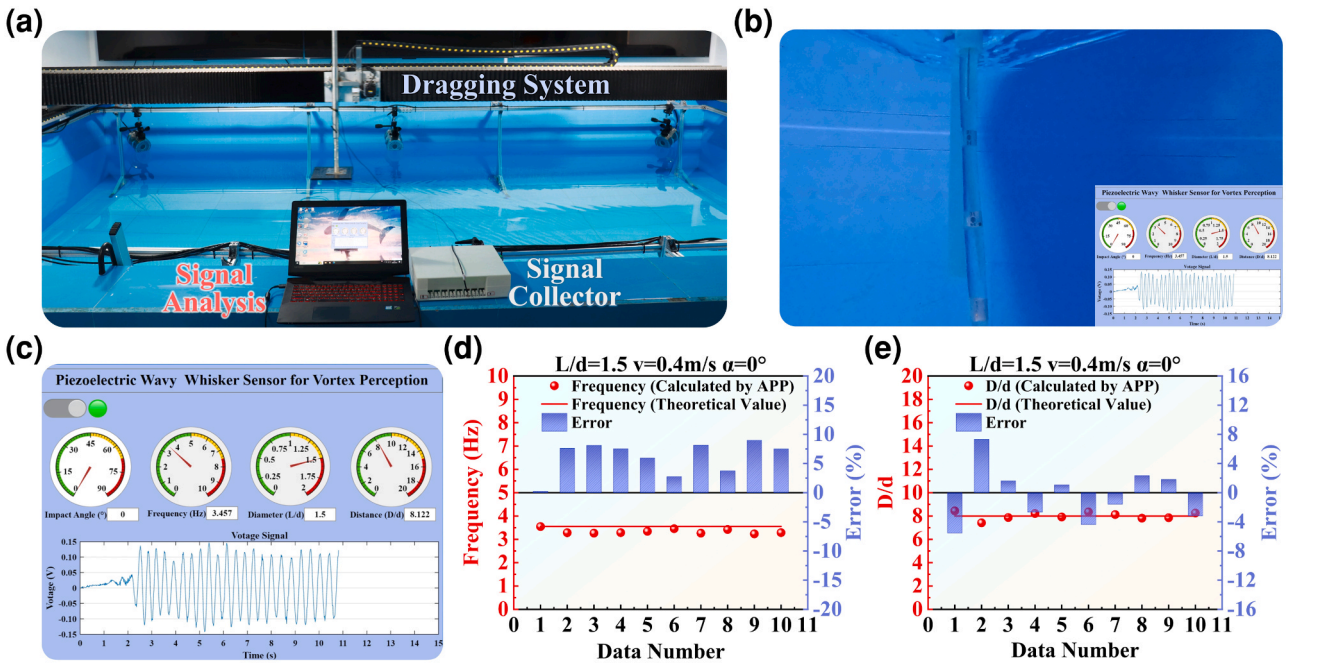

Fig. 7. Vortex perception parameter characterization. (a) Characterization of vortex perception parameters using an app with a real-time display function. (b) The underwater perspective of vortex perception experiment. (c) The calculated value of vortex perception parameters at this moment using the APP. (d) For L/d= 1.5, D/d= 8, v= 0.4 m/s, and α = 0°, the error between the value of the frequency calculated by the APP and the theoretical calculation value. (e) For L/d= 1.5, D/d= 8, v= 0.4 m/s, and α = 0°, the error between the value of the D/d calculated by the APP and the actual value.

middle part of the experimental process is mainly related to the regular disturbance of the PWWS caused by the vortex generated by the bluff body. At this stage, the voltage signal, the values of frequency (f), and distance (D/d) have numerical fluctuations. The error between the value of the frequency (f) calculated by the APP and the theoretical calculation value is less than 10%. The error between the value of distance (D/d) calculated by the APP and the theoretical calculation value (D/d=8) is less than 8%.

Supplementary material related to this article can be found online at.

In this section, we tested an app that can establish real-time communication with the PWWS. At the same time, the APP can establish functional relationships based on the mathematical relationships between various perception parameters in the previous stage of testing. Finally, the APP will output the value of impact angle(α), frequency(f), the dimensionless number ratio between the diameter of the bluff body and the major diameter of the PWWS (L/d), and the dimensionless number distance between the bluff body and the PWWS (D/d). The error between the values of each parameter calculated by the APP and the theoretical calculation values is less than 10%, which also proves that the PWWS as well as the APP has great application value.

4. Conclusion and perspectives

The present study proposed a piezoelectric wavy whisker sensor (PWWS) with a satisfying perceiving ability that can serve as a supplement to underwater perceiving systems. Firstly, the structure and preparation of PWWS are described. Subsequently, this paper studies the relationships between peak voltage & frequency of the PWWS signal and fluid velocity, impact angle, dimensionless diameter of the bluff body plus the dimensionless distance. Results demonstrated peak voltage & frequency are positively correlated to v and α, negatively correlated to L/d, and not correlated to D/d. Moreover, mathematic relationships among the different characteristics of PWWS signal and vortex disturbance are fitted with errors of less than 5%. These correlations and models are proved valid by a theoretical model. Based on the mathematic relationship we established, we formed an APP by MATLAB to conjointly analyse the characteristics of the bluff body and the vortex. For different characteristics of vortex perception, the error between the value calculated by the APP and the theoretical value is less than 10%. In conclusion, the piezoelectric wavy whisker sensor proposed in this article will have potential application value in the field of underwater environment perception.

CRediT authorship contribution statement

Linan Guo: Investigation, Software, Figures, and Writing – review and editing. **Jianhua Liu**: Software, Figures and Writing – review and editing. **Guitao Wu**: Writing – review and editing. **Peng Xu**: Figures and software. **Siyuan Wang**: Investigation and ideas. **Bo Liu:** Visualization, Data analysis and References. **Yuanzheng Li**: Data analysis and References. **Tangzhen Guan**: Figures and software. **Hao Wang**: Writing – review and editing. **Jicang Si**: Figures and Writing – review and editing. **Taili Du**: Conceptualization and Writing – review and editing. **Minyi Xu**: Conceptualization and Writing – review and editing.

Declaration of Competing Interest

The authors declare that they have no known competing financial interests or personal relationships that could have appeared to influence the work reported in this paper.

Data availability

Data will be made available on request.

Acknowledgments

The authors are grateful for the support received from the National Natural Science Foundation of China (52371345), and the Dalian Outstanding Young Scientific and Technological Talents Project (2021RJ11).

Appendix A. Supporting information

Supplementary data associated with this article can be found in the online version at doi:10.1016/j.sna.2023.114875.

References

[1] S. Sendra, J. Lloret, J.Miguel Jimenez, L. Parra, Underwater Acoustic Modems, Ieee Sens. J. 16 (2016) 4063–4071, https://doi.org/10.1109/jsen.2015.2434890.
[2] Z. Yan, P. Gong, W. Zhang, Z. Li, Y. Teng, Autonomous Underwater Vehicle Vision Guided Docking Experiments Based on L-Shaped Light Array, Ieee Access 7 (2019) 72567–72576, https://doi.org/10.1109/access.2019.2917791.
[3] B.G. Gorshkov, K. Yuksel, A.A. Fotiadi, M. Wuilpart, D.A. Korobko, A.A. Zhirnov, et al., Scientific Applications of Distributed Acoustic Sensing: State-of-the-Art Review and Perspective, Sensors 22 (2022), https://doi.org/10.3390/s22031033.
[4] T. Li, S. Rong, X. Cao, Y. Liu, L. Chen, B. He, Underwater image enhancement framework and its application on an autonomous underwater vehicle platform, Opt. Eng. 59 (2020), https://doi.org/10.1117/1.Oe.59.8.083102.
[5] M.R. Arshad, Recent advancement in sensor technology for underwater applications, Indian J. Mar. Sci. 38 (2009) 267–273.
[6] Y. Liu, R. Bao, J. Tao, J. Li, M. Dong, C. Pan, Recent progress in tactile sensors and their applications in intelligent systems, Sci. Bull. 65 (2020) 70–88, https://doi.org/10.1016/j.scib.2019.10.021.
[7] Y. Zou, P. Tan, B. Shi, H. Ouyang, D. Jiang, Z. Liu, et al., A bionic stretchable nanogenerator for underwater sensing and energy harvesting, Nat. Commun. 10 (2019), https://doi.org/10.1038/s41467-019-10433-4.
[8] J. Man, G. Chen, J. Chen, Recent Progress of Biomimetic Tactile Sensing Technology Based on Magnetic Sensors, Biosens. -Basel 12 (2022), https://doi.org/10.3390/bios12111054.
[9] C. Jiang, Q. Li, N. Sun, J. Huang, R. Ji, S. Bi, et al., A high-performance bionic pressure memory device based on piezo-OLED and piezo-memristor as luminescence-fish neuromorphic tactile system, Nano Energy 77 (2020), https://doi.org/10.1016/j.nanoen.2020.105120.
[10] M. Asadnia, A.G.P. Kottapalli, J. Miao, M.E. Warkiani, M.S. Triantafyllou, Artificial fish skin of self-powered micro-electromechanical systems hair cells for sensing hydrodynamic flow phenomena, J. R. Soc. Interface 12 (2015), https://doi.org/10.1098/rsif.2015.0322.
[11] X. Hu, Y. Jiang, Z. Ma, Y. Xu, D. Zhang, Bio-inspired Flexible Lateral Line Sensor Based on P(VDF-TrFE)/BTO Nanofiber Mat for Hydrodynamic Perception, Sensors 19 (2019), https://doi.org/10.3390/s19245384.
[12] G. Liu, A. Wang, X. Wang, P. Liu, A Review of Artificial Lateral Line in Sensor Fabrication and Bionic Applications for Robot Fish, Appl. Bionics Biomech. 2016 (2016), https://doi.org/10.1155/2016/4732703.
[13] M.-A. Sayegh, H. Daraghma, S. Mekid, S. Bashmal, Review of Recent Bio-Inspired Design and Manufacturing of Whisker Tactile Sensors, Sensors 22 (2022), https://doi.org/10.3390/s22072705.
[14] T. Shizhe, Underwater artificial lateral line flow sensors, Microsyst. Technol. -Micro- Nanosyst. -Inf. Storage Process. Syst. 20 (2014) 2123–2136, https://doi.org/10.1007/s00542-014-2350-1.
[15] Y. Jiang, Z. Ma, D. Zhang, Flow field perception based on the fish lateral line system, Bioinspiration Biomim. 14 (2019), https://doi.org/10.1088/1748-3190/ab1a8d.
[16] W. Hanke, M. Witte, L. Miersch, M. Brede, J. Oeffner, M. Michael, et al., Harbor seal vibrissa morphology suppresses vortex-induced vibrations, J. Exp. Biol. 213 (2010) 2665–2672, https://doi.org/10.1242/jeb.043216.
[17] H. Hans, J.M. Miao, M.S. Triantafyllou, Mechanical characteristics of harbor seal (Phoca vitulina) vibrissae under different circumstances and their implications on its sensing methodology, Bioinspiration Biomim. 9 (2014), https://doi.org/10.1088/1748-3182/9/3/036013.
[18] N. Schulte-Pelkum, S. Wieskotten, W. Hanke, G. Dehnhardt, B. Mauck, Tracking of biogenic hydrodynamic trails in harbour seals (Phoca vitulina), J. Exp. Biol. 210 (2007) 781–787, https://doi.org/10.1242/jeb.02708.
[19] T. Adachi, Y. Naito, P.W. Robinson, D.P. Costa, L.A. Huckstadt, R.R. Holser, et al., Whiskers as hydrodynamic prey sensors in foraging seals, Proc. Natl. Acad. Sci. USA 119 (2022), https://doi.org/10.1073/pnas.2119502119.
[20] F.E. Fish, L.E. Howle, M.M. Murray, Hydrodynamic flow control in marine mammals, Integr. Comp. Biol. 48 (2008) 788–800, https://doi.org/10.1093/icb/icn029.
[21] K. Lyons, C.T. Murphy, J.A. Franck, Flow over seal whiskers: Importance of geometric features for force and frequency response, Plos One 15 (2020), https://doi.org/10.1371/journal.pone.0241142.
[22] H.R. Beem, M.S. Triantafyllou, Wake-induced 'slaloming' response explains exquisite sensitivity of seal whisker-like sensors, J. Fluid Mech. 783 (2015) 306–322, https://doi.org/10.1017/jfm.2015.513.
[23] X. Zheng, A.M. Kamat, M. Cao, A.G.P. Kottapalli, Wavy Whiskers in Wakes: Explaining the Trail-Tracking Capabilities of Whisker Arrays on Seal Muzzles, Adv. Sci. 10 (2023), https://doi.org/10.1002/advs.202203062.
[24] J.Z. Gul, K.Y. Su, K.H. Choi, Fully 3D Printed Multi-Material Soft Bio-Inspired Whisker Sensor for Underwater-Induced Vortex Detection, Soft Robot. 5 (2018) 122–132, https://doi.org/10.1089/soro.2016.0069.
[25] G. Liu, Y. Jiang, P. Wu, Z. Ma, H. Chen, D. Zhang, Artificial Whisker Sensor with Undulated Morphology and Self-Spread Piezoresistors for Diverse Flow Analyses, Soft Robot. 10 (2023) 97–105, https://doi.org/10.1089/soro.2021.0166.
[26] H. Beem, M. Hildner, M. Triantafyllou, Ieee, Characterization of a harbor seal whisker-inspired flow sensor, MTS/IEEE Oceans Conference,, 2012.
[27] X. Zheng, A.M. Kamat, A.O. Krushynska, M. Cao, A.G.P. Kottapalli, 3D Printed Graphene Piezoresistive Microelectromechanical System Sensors to Explain the Ultrasensitive Wake Tracking of Wavy Seal Whiskers, Adv. Funct. Mater. 32 (2022), https://doi.org/10.1002/adfm.202207274.
[28] X. Zhang, X. Shan, T. Xie, J. Miao, H. Du, R. Song, Harbor seal whisker inspired self-powered piezoelectric sensor for detecting the underwater flow angle of attack and velocity, Measurement 172 (2021), https://doi.org/10.1016/j.measurement.2020.108866.
[29] S. Wang, P. Xu, X. Wang, J. Zheng, X. Liu, J. Liu, et al., Underwater bionic whisker sensor based on triboelectric nanogenerator for passive vortex perception, Nano Energy 97 (2022), https://doi.org/10.1016/j.nanoen.2022.107210.
[30] H.R. Beem, Passiv. wake Detect. Using Seal. whisker-inspired Sens. (2015).
[31] M.J. David, M. Mathur, R.N. Govardhan, J.H. Arakeri, The kinematic genesis of vortex formation due to finite rotation of a plate in still fluid, J. Fluid Mech. 839 (2018) 489–524, https://doi.org/10.1017/jfm.2017.908.
[32] P.G. Saffman, Vortex Dynamics, Cambridge University Press,, Cambridge, 1993 https://doi.org/DOI: 10.1017/CBO9780511624063.
[33] X. Shan, R. Song, B. Liu, T. Xie, Novel energy harvesting: A macro fiber composite piezoelectric energy harvester in the water vortex, Ceram. Int. 41 (2015) S763–S767, https://doi.org/10.1016/j.ceramint.2015.03.219.
[34] B. Balachandran, E.B. Magrab. Vibrations, 3 ed..,, Cambridge University Press,, Cambridge, 2018 https://doi.org/DOI: 10.1017/9781108615839.
[35] A.E. Cohen, R.R. Kunz, Large-area interdigitated array microelectrodes for electrochemical sensing, Sens. Actuators B-Chem. 62 (2000) 23–29, https://doi.org/10.1016/s0925-4005(99)00372-x.
[36] D.W. Jin, Y.J. Ko, C.W. Ahn, S. Hur, T.K. Lee, D.G. Jeong, et al., Polarization- and Electrode-Optimized Polyvinylidene Fluoride Films for Harsh Environmental Piezoelectric Nanogenerator Applications, Small 17 (2021), https://doi.org/10.1002/smll.202007289.
[37] M. Zhang, T. Gao, J. Wang, J. Liao, Y. Qiu, Q. Yang, et al., A hybrid fibers based wearable fabric piezoelectric nanogenerator for energy harvesting application, Nano Energy 13 (2015) 298–305, https://doi.org/10.1016/j.nanoen.2015.02.034.

Linan Guo is currently pursuing the master's degree in Dalian Maritime University, China. His current research work focuses on Triboelectric Nanogenerator and the bionic whisker sensor based on the triboelectric nanogenerators.

Jianhua Liu is currently pursuing the master's degree in Dalian Maritime University, China. His current research interests include underwater robot tactile system and triboelectric nanogenerator.

Guitao Wu graduated from Dalian Maritime University with a doctor's degree in marine engineering in 2005. He has been a professor in Dalian Maritime University since 2007, mainly engaged in the research work of modern marine engineering management. His research focuses on intelligent ships, green ships as well as energy capture and self-driving sensing based on triboelectric nanogenerators.

Peng Xu is currently pursuing his doctor degree in Dalian Maritime University, China. His current research interests include self-powered sensing system and control, bio-inspired design and control for marine and underwater robots and triboelectric nanogenerators.

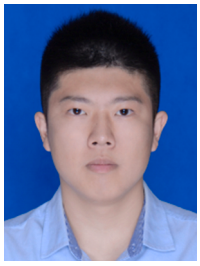

Siyuan Wang is currently pursuing his doctor degree in Dalian Maritime University, China. His current research interests in the self-powered sensing system and application, bionic sensors and triboelectric nanogenerators.

Bo Liu is currently pursuing the master's degree in Dalian Maritime University, China. His current research interests include self-powered sensing system and triboelectric nanogenerators.

Yuanzheng Li is pursuing the master's degree in Dalian Maritime University, China. His current research interests are the Underwater tactile sensor based on triboelectric nanogenerator.

Tangzhen Guan is currently pursuing the Master's degree in Technical Institute of Physics and Chemistry, Chinese Academy of Sciences. His current research interests in frontiers in Liquid Metal-based Flexible Intelligent Sensing.

Hao Wang received his Ph.D. degree from Texas A&M University. Now he is an associate professor in Marine engineering College, Dalian Maritime University. His research interests include motion simulation, improvement, and stability analysis of the wave energy harvester.

Jicang Si received his Ph.D. degree in Energy and Resources Engineering from Peking University in 2023. Now he is a Lecturer in the Marine Engineering College, Dalian Maritime University. His current research is mainly focused on the areas of blue energy, turbulent flow and combustion.

Taili Du has been with Dalian Maritime University where he is currently an Associate Professor since 2010. He received his B. S. and M.S. from Dalian Maritime University in China in 2008 and 2010, and he is as a doctoral candidate in Marine Engineering College, Dalian Maritime University. His current research work focuses on vibration energy harvesting and self-powered vibration sensor based on Triboelectric Nanogenerator.

Minyi Xu received his Ph.D. degree from Peking University in 2012. During 2016–2017, he joined Professor Zhong Lin Wang' group at Georgia Institute of Technology. Now he is a Professor in the Marine Engineering College, Dalian Maritime University. His current research is mainly focused on the areas of blue energy, self-powered systems, triboelectric nanogenerators and its practical applications in smart ship and ocean.